Neurobiology of Disease 67 (2014) 165–179

Contents lists available at ScienceDirect

Neurobiology of Disease

journal homepage: www.elsevier.com/locate/ynbdi

Long-lasting significant functional improvement in chronic severe spinal cord injury following scar resection and polyethylene glycol implantation

Veronica Estrada [a], Nicole Brazda [a], Christine Schmitz [a], Silja Heller [a], Heinrich Blazyca [b], Rudolf Martini [b], Hans Werner Müller [a,*]

[a] Molecular Neurobiology Laboratory, Department of Neurology, Heinrich-Heine-University Medical Center Düsseldorf, Moorenstr. 5, 40225 Düsseldorf, Germany
[b] Department of Neurology, Developmental Neurobiology, University Medical Center Würzburg, Josef-Schneider-Str. 11, 97080 Würzburg, Germany

ARTICLE INFO

Article history:
Received 28 January 2014
Revised 17 March 2014
Accepted 28 March 2014
Available online 5 April 2014

Keywords:
Trauma
Axon regeneration
Biomatrix
Complete spinal cord transection
Chronic Spinal Cord Injury
Locomotor improvement
Cell invasion
Schwann cell
Remyelination
Scar resection

ABSTRACT

We identified a suitable biomatrix that improved axon regeneration and functional outcome after partial (moderate) and complete (severe) chronic spinal cord injury (SCI) in rat. Five weeks after dorsal thoracic hemisection injury the lesion scar was resected *via* aspiration and the resulting cavity was filled with different biopolymers such as Matrigel™, alginate-hydrogel and polyethylene glycol 600 (PEG) all of which have not previously been used as sole graft-materials in chronic SCI. Immunohistological staining revealed marked differences between these compounds regarding axon regeneration, invasion/elongation of astrocytes, fibroblasts, endothelial and Schwann cells, revascularization, and collagen deposition. According to axon regeneration-supporting effects, the biopolymers could be ranked in the order PEG >> alginate-hydrogel > Matrigel™. Even after complete chronic transection, the PEG-bridge allowed long-distance axon regeneration through the grafted area and for, at least, 1 cm beyond the lesion/graft border. As revealed by electron microscopy, bundles of regenerating axons within the matrix area received myelin ensheathment from Schwann cells. The beneficial effects of PEG-implantation into the resection-cavity were accompanied by long-lasting significant locomotor improvement over a period of 8 months. Following complete spinal re-transection at the rostral border of the PEG-graft the locomotor recovery was aborted, suggesting a functional role of regenerated axons in the initial locomotor improvement. In conclusion, scar resection and subsequent implantation of PEG into the generated cavity leads to tissue recovery, axon regeneration, myelination and functional improvement that have not been achieved before in severe chronic SCI.

Introduction

Spinal cord injury (SCI) generally results in life-long severe impairments for the patients. Present research in the field of SCI largely targets acute SCI. However, the majority of SCI patients are those with chronic lesions who may benefit insufficiently from therapeutic treatments designed for acute application. Compared to treatments of acute experimental SCI, the efficacy of therapies promoting axonal regeneration seems impaired in chronic models (Houle and Tessler, 2003). Accumulation of growth-inhibitory molecules associated with central myelin (Buchli and Schwab, 2005; Cafferty and Strittmatter, 2006; Filbin, 2003) or the lesion scar (Fawcett, 2006; Klapka and Muller, 2006; Silver and Miller, 2004) could be responsible for regeneration failure in both acute and chronic SCI. Using iron chelators to inhibit collagen-biosynthesis we have previously demonstrated the beneficial effects of transient suppression of fibrous scarring in an acute SCI model (Klapka et al., 2005; Schiwy et al., 2009). However, since iron chelators suppress the formation of fibrotic scarring but do not degrade an existing scar, this treatment is not transferable to chronic SCI where a mature lesion scar, with a plethora of axon growth-inhibitory molecules attached (Bundesen et al., 2003; Davies et al., 2004; Niclou et al., 2006), has already formed. Careful surgical resection of the scar and filling-in of scaffolding matrices into the resulting cavity could be a possible option for a regeneration-supporting therapy in chronic SCI.

Here we describe a chronic (5 weeks) SCI and scar resection model in rat, and different viscous matrix materials in regard to their ability to support axon regeneration. As shown previously, the scar is fully developed at the injury site after this time while the biosynthesis of most

Abbreviations: HX, hemisection; TX, complete transection; RX, scar resection; ALG, alginate-hydrogel; MG, Matrigel™; PEG, polyethylene glycol; mBBB, modified BBB open field test; wpl, week post lesion; wpr, week post resection; dpReTX, days post axonal re-transection; rT, rostral tracing; Ax, axon, As, astrocyte; Bv, blood vessel; Fi, fibroblastic cell; Sc, Schwann cell.

* Corresponding author at: Molecular Neurobiology Laboratory, Department of Neurology, Heinrich-Heine-University Medical Center Düsseldorf, Moorenstr. 5, 40225 Düsseldorf, Germany.
E-mail address: hanswerner.mueller@uni-duesseldorf.de (H.W. Müller).
Available online on ScienceDirect (www.sciencedirect.com).

http://dx.doi.org/10.1016/j.nbd.2014.03.018
0969-9961/

scar-associated CSPGs has subsided (Tang et al., 2003) and spontaneous behavioral recovery has reached its plateau (Ung et al., 2007). For cavity-filling after scar resection we chose three biopolymers: (i) Matrigel™ (MG), (ii) alginate-hydrogel (ALG) and (iii) polyethylene glycol 600 (PEG).

These materials were chosen because of their reported beneficial effects in the treatment of acute SCI: MG is a gel obtained from the Engelbreth–Holm–Swarm sarcoma and has been described as a suitable gel matrix for tissue regeneration (Cassell et al., 2001) and axon growth (Tonge et al., 1997). ALG is a polysaccharide distributed widely in the cell walls of brown algae and has previously been applied as a cell carrier substance in SCI research to promote axonal regeneration and elongation, both *in vitro* and *in vivo* (Kataoka et al., 2004; Novikov et al., 2002, 2006). Application of PEG successfully yielded repair of crushed as well as transected spinal cord axons leading to immediate recovery of axonal conduction in an acute injury model (Borgens et al., 2002; Shi and Borgens, 2000). It should be noted that both terms "biomatrix" and "biopolymer" have been used to describe these materials because there is no generally accepted definition for either term. MG and ALG are often called as either biomatrices or biopolymers. By the broad definition of a biomatrix as a biological or biochemical matrix PEG can also be termed a biomatrix, but because of the lack of a cross-linking reaction we prefer to use the term "biopolymer" for PEG. We found the latter term more suitable than "biomatrix", because PEG is considered a technical biopolymer showing biodegradability and compatibility with biological tissue.

The present investigation is, to our knowledge, the first that directly compared MG, ALG and PEG with respect to their suitability as regeneration-supporting matrix materials in animal models of chronic moderate and complete SCI. We have investigated and compared spinal cord tissue responses to these biopolymers with respect to axon regeneration, cell invasion, vascularization and functional locomotor outcome. We could identify and select PEG as a highly suitable biopolymer-matrix which supports glial cell invasion, neovascularization as well as regeneration of myelinated axons into and beyond the lesion zone leading to a significant degree of improvement of locomotor behavior that has not been matched or outbalanced by any other treatment of complete chronic SCI.

Materials & methods

Surgery procedures

During all surgical procedures animals were placed on a heating pad to maintain body temperature. The timelines in Supplementary Fig. 1 provide an overview of the experimental procedures.

Spinal cord injury

Dorsal hemisection lesion model (HX, Supplementary Fig. 1A): Lesioning was performed according to a modification of a previously published protocol (Schiwy et al., 2009). In brief, adult female Wistar rats (HanTac:WH; Taconic) weighing 200–230 g were anesthetized with isoflurane (Forene, Abbott; 2–3% in O_2 and N_2O at a ratio of 1:2). Following laminectomy at thoracic level Th8/9 and opening of the *dura mater* via a longitudinal cut, a dorsal hemisection injury was performed with a Scouten wire knife (Bilaney). After suture of the *dura mater* the lesion area was covered with a piece of Elvax copolymer (ethylene vinyl acetate; a gift from Erbslöh GmbH) or with a small piece of a thermoplastic polymer (Nescofilm®, Roth). Finally, the overlying muscles and skin were sutured in layers, and the animals were housed with food and water *ad libitum*. Post-operative care included prophylactic daily oral Baytril™ (Bayer Health Care) administration for one week. Animals received daily manual bladder expression when necessary. They were inspected for signs of infection, dehydration or automutilation with appropriate veterinary assistance as needed. Institutional guidelines for animal safety and comfort were adhered to, and all surgical interventions and pre- and post-surgical animal care were provided in compliance with the German Animal Protection law (State Office, Environmental and Consumer Protection of North Rhine-Westphalia, LANUV NRW).

Complete transection model (TX, Supplementary Fig. 1B): Following laminectomy the *dura* at Th8/9 was opened with a traverse cut and the spinal cord was slightly lifted and separated from the dura with a spinal cord hook (Fine Science Tools). The spinal cord was completely transected by a traverse cut with a pair of micro-scissors which resulted in the retraction of the transected cord leaving a small gap between the two segments. Two small spatulas were used to carefully pull the segments apart to ensure complete transection. After suture of the *dura mater* the lesion area was covered with a small piece of Nescofilm®, and overlying tissues were sutured in layers. Housing and post-operative care were performed as mentioned above.

Spinal cord re-transection (ReTX) at 8 months post-resection (mpr): One week prior to sacrifice, the spinal cord was completely re-transected at the rostral border of the graft following laminectomy at Th7 in a small group of PEG-treated animals ($n = 3$). TX only-controls did not undergo this procedure because they did not show any noteworthy spontaneous recovery as revealed by their generally low mBBB scores. After one week post ReTX the animals underwent mBBB open field testing. The one week post ReTX time point was chosen for locomotor testing in order to exclude the possibility that an observed disappearance of the locomotor recovery upon ReTX is merely a result of spinal shock.

Scar resection and matrix insertion

Five weeks after the initial SCI, animals were randomly assigned into the respective treatment groups. Animals of the RX-groups were re-anesthetized and the lesion area was re-opened. The Nescofilm® cover was removed and the sutures were cut open to expose the lesioned spinal cord. Two incisions, one above and one below the spinal cord lesion were made at a distance of 4 mm apart from each other with a pair of micro-scissors. Spinal cord tissue was removed via aspiration with a small pipette connected to a vacuum pump (Supplementary Fig. 2).

The region between the two incisions was aspirated until the central canal became visible (hemisection) or until all scar tissue (recognizable by its stiff texture) was removed, respectively. The tested matrix materials were injected with a 10 µl Hamilton syringe (#701 LT) equipped with a blunt canula using a stereotactic device. Aliquots of Matrigel™ (BD Biosciences) were thawed on ice for liquefaction. For Matrigel (MG) injection, cooled instruments were used in order to prevent premature gel formation. For alginate-hydrogel (ALG) preparation, a 2% (w/v) solution of alginate (Pronova UP LVM; NovaMatrix) in 150 mM sodium chloride (NaCl) was filtered with a sterile syringe filter. The alginate was set by exposure to 0.1 M calcium chloride ($CaCl_2$) resulting in a viscous hydrogel. For chelator-containing ALG solution, first a solution of 40 mM iron chelator [2,2′-bipyridine]-5,5′-dicarboxylic acid (BPY-DCA) and 150 mM NaCl in H_2O was prepared. Via addition of 2% (w/v) alginate powder and subsequent filtration, an injectable ALG was created. PEG (Merck) was heated to 37 °C prior to implantation to allow liquefaction. Application of low molecular weight PEG such as PEG 600 is safe as it is almost completely absorbed and excreted in urine (European Food Safety Authority, 2006). Systemic administration of PEG has previously been described to successfully yield repair of crushed as well as transected spinal cord axons leading to immediate recovery of axonal conduction in an acute injury model (Borgens et al., 2002; Shi and Borgens, 2000). Prior to this study, we tested PEGs of different molecular weights (PEG 400, PEG 600, PEG 1000, and an aqueous solution of PEG 2000). In addition to chemical cues, mechanical stimuli could also influence neuronal growth. PEG 600 proved to be the most suitable PEG for the intended purpose, whereas the viscosity of the

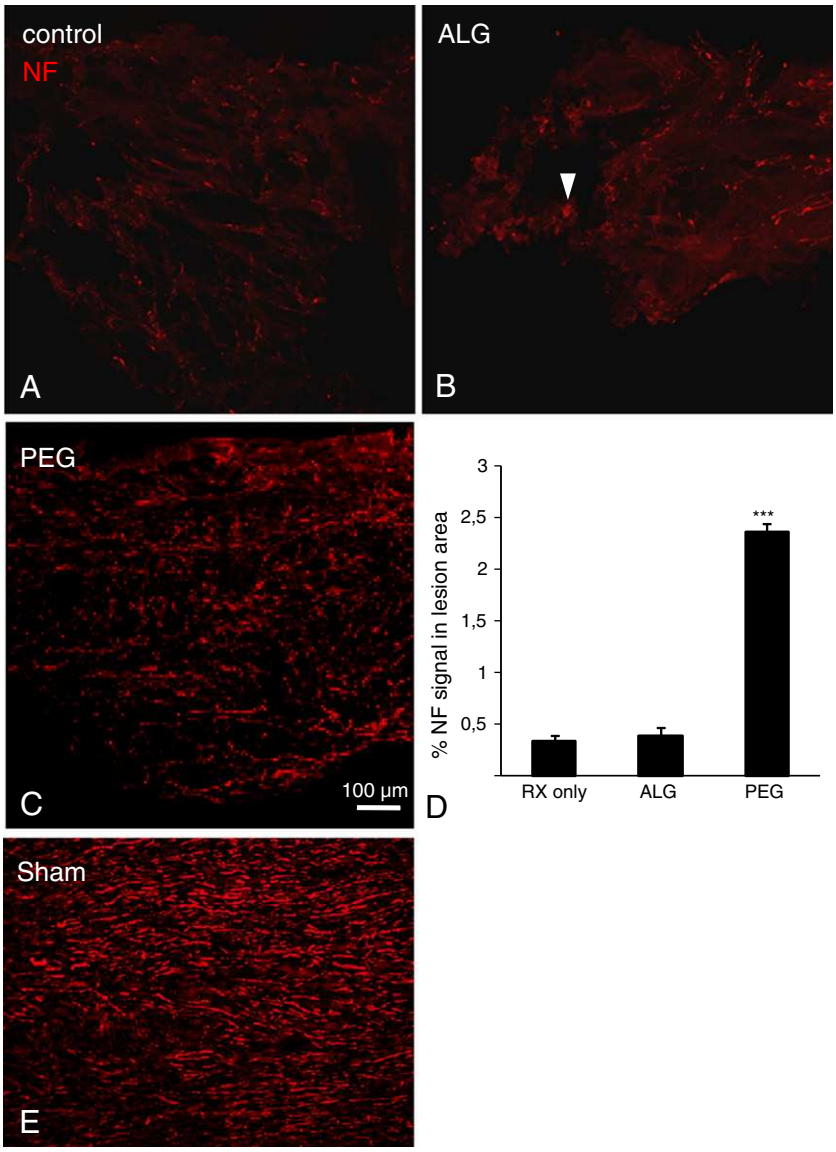

Fig. 1. Investigation of spontaneous axonal regeneration into the HX lesion/matrix area via NF-IR at 5 wpr. NF-IR in the lesion area of "control" (RX only)- (A), ALG- (B) and PEG- (C) treated animals. (A–C): Representative images of the IF-stained lesion area in sagittal sections of the lesion area. (D): Results of quantification of NF-signal (after background elimination) in the lesion area via semi-automated analysis using the Image J plug-in Feature J. Bars represent mean + SEM. Spontaneous axonal ingrowth into the lesion area was highly significantly increased after insertion of PEG ($n = 64$) compared to ALG ($n = 53$) or RX only ($n = 12$). No statistical differences were found between ALG- and RX only-controls. Arrowhead in (B): exemplary structure or area, respectively, exhibiting great extent of nonspecific NF-IR, but hardly any neuronal morphology. Such structures were eliminated in the course of background elimination and were not considered in the final quantification. Statistics in (D): Kruskal–Wallis and post-hoc Mann–Whitney *U*-test with Holm–Bonferroni correction. $^{*}p \leq 0.05$, $^{**}p \leq 0.01$, $^{***}p \leq 0.001$. E: NF-IR in the equivalent region of a sham animal is shown for comparison. 50 µm-sections.

other tested PEGs was found to be either too low (extensive leakage of PEG 400 and of the aqueous solution of PEG 2000) or too high (encapsulation of PEG 1000). After filling of the cavity with the respective biopolymer, the lesion area was covered with a *dura* replacement material (Nescofilm® polymer [Roth] or Neuro-Patch® [Braun], respectively) which was affixed to surrounding tissue with tissue glue to prevent extensive leakage of the filling materials. The effect of Neuro-Patch® (a clinically used cell-permeable dura replacement material) as a coverage of the implant area was compared to those of the non-permeable Nescofilm® in PEG-animals. Although it is described by the company to support the integration of endogenous fibroblasts while minimizing the risk of inflammation no differences could be detected with the applied analytic methods (*i.e.*, no changes in cell infiltration of the implant or in scarring, respectively). This may be explained either by the severity of the procedure and the large dural defect or by the nature of the PEG, respectively. Of note, BPY-DCA could not be resolved in PEG 600 without further dilution of the polymer which, in turn, would reduce viscosity and thus unfavorably alter the properties of PEG 600. Overlying muscle and skin were sutured in layers, and the animals were housed with food and water *ad libitum*. For postoperative care and animal safety guidelines see above.

Control animals either received the initial lesion only but no scar resection ("lesion only"), respectively, or they received, in addition, a scar resection without matrix injection ("RX only").

Anterograde corticospinal tract tracing

After craniotomy the corticospinal tract (CST) was anterogradely traced via multiple small volume injections (0.2 µl each) of biotinylated dextran amine (BDA; 10,000 MW, 10%; Molecular Probes) into the brain of anesthetized animals. Eight injections were made stereotactically (Kopf stereotactic frame) into the sensorimotor cortex of each hemisphere using the coordinates previously described (Klapka et al.,

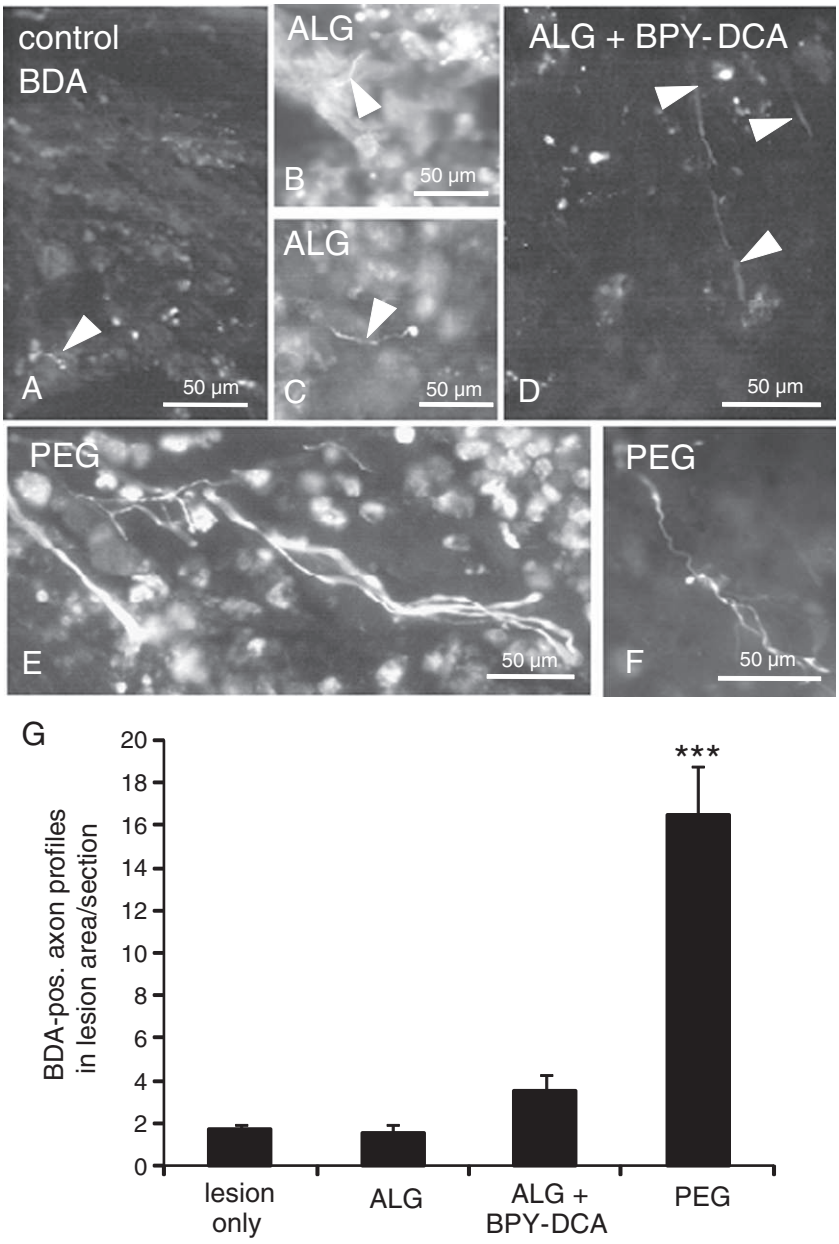

Fig. 2. Investigation of spontaneous axonal regeneration into the HX lesion/matrix area via anterograde BDA-labeling at 5 wpr. Spontaneous axonal regeneration of BDA-labeled axons into the lesion area of lesion only- (A), ALG- (B,C), ALG + BPY-DCA- (D) and PEG- (E,F) treated animals at 5 wpr (lesion only-controls: 10 wpl). (A–F): representative images of BDA- positive structures in the lesion area in 50 µm sagittal sections of controls, ALG-, ALG + BPY-DCA-, and PEG-treated animals. Arrowheads in (A–D): BDA-positive axonal structures. (G): Quantification by counting of BDA-positive axon fragments in lesion. Bars represent mean + SEM. Spontaneous axonal regeneration into lesion area was highly significantly increased in PEG ($n = 31$) compared to ALG ($n = 35$), ALG + BPY ($n = 39$) or lesion only ($n = 46$). Positive trend in the comparison of ALG + BPY-DCA with lesion only-controls. Statistics in (G): Kruskal–Wallis and post-hoc Mann–Whitney *U* test with Holm–Bonferroni correction. $^{***}p \leq 0.001$.

2005). Anterograde CST tracing was performed three weeks prior to sacrifice (Supplementary Fig. 3).

Rostral labeling of descending axons in the thoracic spinal cord

BDA was injected into the spinal cord 3 mm rostrally to the lesion/implantation site of anesthetized animals. Injections (0.2 µl each) of BDA were applied: In the midline at a depth of 1.5 mm (ventral funiculus), 0.8 mm (dorsal CST), and 0.5 mm (cuneate and gracile funiculi) from the *pia mater*, and at 1.0 mm laterally from the midline on each side at depths of 1.2, 0.8 and 0.4 mm (lateral funiculi) from the *pia mater* using a grease-sealed glass canula attached to a Hamilton syringe. Rostral BDA-tracing was performed one week prior to sacrifice (Supplementary Fig. 3).

Anterograde labeling of ascending sensory axons

Animals were anesthetized and the sciatic nerve was exposed at mid-thigh level. A ligature (Vicryl 4–0, Ethicon) was loosely placed proximal from the origin of the tibial and peroneal nerves. A small incision was made in the epineurium distal to the ligature. The tip of a glass canula sealed to a Hamilton syringe was inserted through the incision and 3.5 µl of a 1% cholera toxin B subunit solution (CTB; List Biological Laboratories) were slowly injected over a 3 min time period. Following the injection the glass needle was left in place for 4 min to prevent leakage of CTB. After this time, the syringe was removed and the ligature was further tightened around the nerve. Finally, the nerve was crushed with a pair of fine forceps for 10 s proximal to the injection site to allow sufficient uptake of CTB. After this procedure, overlying tissues were

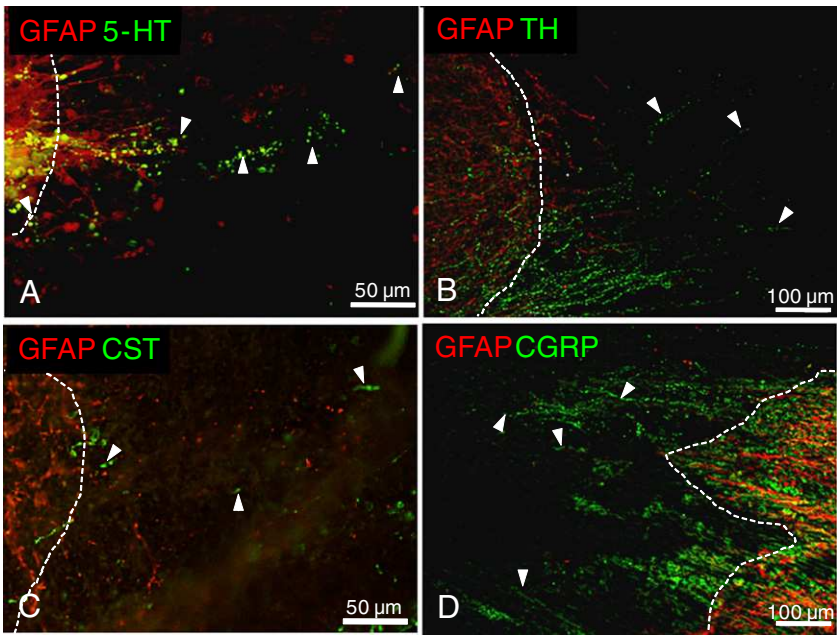

Fig. 3. Characterization of regenerating axon populations in the PEG-matrix (HX) at 5 wpr. Axons from all analyzed fiber populations were able to regenerate into a chronic SCI scar removal site filled with PEG 600. Examined axonal populations in the PEG-matrix area in 50 µm sagittal sections were serotonergic axons identified via 5-hydroxytryptamine-IR (5-HT, A), catecholaminergic axons identified via tyrosine hydroxylase-IR (TH; B), the CST (C), and sensory axons expressing calcitonin gene-related peptide (CGRP, D). Arrowheads: positively stained axonal structures (green) in the matrix area. Note also GFAP-positive (red) structures invading the lesion site. Orientation of sections: rostral — left, caudal — right.

sutured in layers. Both sciatic nerves of an animal were labeled following this protocol. Anterograde labeling of ascending sensory fibers was performed five days prior to sacrifice (Supplementary Fig. 3).

Tissue preparation

Tissue preparation for immunohistochemistry and axon tracing was performed as previously described (Klapka et al., 2005; Schiwy et al., 2009). In brief, the animals were anesthetized with Narcoren® (Merial) and transcardially perfused with ice-cold phosphate-buffered saline (PBS) for two minutes and subsequently with 4% paraformaldehyde (PFA; Merck) for 15 min. Spinal cords were post-fixed in 4% paraformaldehyde at 4 °C. Spinal cord pieces containing the lesion area were either embedded and cut in paraffin (10 µm parasagittal sections), or they were cryopreserved in 30% sucrose at 4 °C to be cut on a cryostat (10 µm parasagittal sections or 10 µm cross sections, respectively) or on a freezing microtome (40–50 µm parasagittal free-floating sections). Lesion/matrix area-containing sections from ALG-treated animals were collected in $CaCl_2$-containing (100 mM) PBS solution. Due to ALG's susceptibility to impurity, NaN_3 (0.1%) was added to the tissue collecting solution.

Immunohistochemistry

In the hemisection studies which were conducted to histologically analyze the lesion area and to compare the effects of the applied materials immunohistochemical analyses were performed at the time points five weeks post lesion (5 wpl; this time point represents the status at the time of scar resection in the treated animals), one week post scar resection (1 wpr) and five weeks post scar resection (5 wpr), respectively. The 1 wpr time point was considered a highly interesting time point regarding the cellular invasion into the lesion area because at this early time point strong differences in the efficacy of the tested materials were already apparent in the neurofilament staining. For the qualitative analysis of the axonal regeneration into the lesion area the 5 wpr time point was chosen to allow a more substantial axon growth. Control animals without scar resection were analyzed for cell invasion of the lesion area at 1 wpl or 5 wpl to either compare the results of the chronic scar resection at 1 wpr with the acute situation (1 wpl; Col 4, GFAP, P-4-H, S100) or with the chronic situation prior to the removal of the scar tissue (5 wpl, Col 4, GFAP, vWF).

Immunohistochemical staining of paraffin sections was preceded by deparaffinization procedures, and standard immunohistological protocols were used for all staining procedures. Untreated sections and no-primary antibody controls were analyzed for evidence of autofluorescence. The following antibodies directed to the proteins mentioned were used: SMI312 (pan-axonal marker of phosphorylated neurofilament [NF]; Covance, 1:1000), glial fibrillary acidic protein (GFAP; Chemicon/Millipore, 1:350), rat prolyl 4-hydroxylase (P-4-H; Acris, 1:200), NG2 (Chemicon, 1:100), *adenomatous polyposis coli* (APC, clone CC-1; Calbiochem, 1:100), ED1 (Serotec, 1:1000), myelin basic protein (MBP; Chemikon/Millipore, 1:50), glial fibrillary acidic protein (GFAP; Dako, 1:1000), 5-hydroxytryptamine (5-HT; Biologo, 1:30), tyrosine hydroxylase (TH; Abcam, 1:750), von Willebrand factor (vWF; Dako, 1:1000), S100β (S100; Sigma, 1:200), calcitonin gene-related peptide (CGRP; Serotec, 1:1500), cholera toxin β subunit (CTB; List, 1:80,000), collagen type IV (Col4; Biodesign), PDGF receptor α (PDGFra; Santa Cruz, 1:300), and PDGF receptor β (PDGFrb; Abcam, 1:100). Reduction of aldehyde groups with $NaBH_4$ was used for P-4-H, NG2 and APC, epitope retrieval with citrate buffer was used for MBP, and epitope retrieval with protease was used for vWF and Col4.

Sections were stained with one of the antibodies listed above by standard immunohistological protocols: Washing with PBS, blocking with 5% normal donkey serum or with 5% normal goat serum, respectively, for 1 h at room temperature, incubation with first antibody in PBS/5% normal serum overnight (or, in the case of CTB, for 65 h, respectively) at 4 °C, washing with PBS and incubation with Alexa 488 or 594-conjugated secondary antibody (Molecular Probes), respectively. For triple staining, an additional biotinylated second antibody was visualized with streptavidin Alexa 405 (Molecular Probes). For BDA-visualization of anterogradely labeled axons Oregon Green® 488 (Molecular Probes; 1:1000) was applied.

In the case of DAB-staining visualization of 3,3′-diaminobenzidine (DAB) was performed after incubation of the sections with the second antibody followed by incubation with avidin–biotin complex (ABC; Vector Laboratories).

Quantification of axon profile density or axon numbers

For quantification of axon density or axon numbers in the lesion area, at least 8–12 fifty-μm serial spinal cord parasagittal sections per animal were analyzed. The number of stained sections for the RX only-control group was limited to three sections per animal because of the observed consistent lack of regenerated tissue in the resection area. The scar area was defined by lack of immune reactivity (IR) to GFAP antibody and/or by lack of Sudan Black B (Fluka) myelin staining. Spinal cord sections with DAB antibody visualization or with Alexa 488-, Alexa 594- or Alexa 405-coupled secondary antibodies, respectively, were analyzed using a BZ-8000 Keyence digital microscope. Quantification of BDA-labeled axons (Oregon Green® visualization of BDA) after tracer injection into the spinal cord rostral to the injury was carried out using a Nikon Diaphot 300 fluorescent microscope. Quantitative analysis of NF-positive axons in the lesion area was performed using a Zeiss LSM 510 confocal laser scanning microscope. Three laser lines emitting at 405, 488 and 543 nm were used to excite 4′,6-Diamidin-2′-phenylindol-dihydrochlorid (DAPI), Alexa 405, Alexa 488 and Alexa 594, respectively. Digitalized pictures were saved in TIF-format. Quantification of NF-positive axon profile density was performed using graphics editing software. NF-IR was used to identify axon profiles. GFAP-antibody was used to label reactive astrocytes and to delineate the borders of the fibrous lesion scar. Images of NF-IR of the entire lesion area (defined by lack of GFAP-IR) of all sections analyzed were taken using the 10×-objective of a Zeiss LSM 510 confocal microscope in the focal plane with the highest NF-IR intensity. Attention was given to ensure identical settings for laser intensity, scan speed, amplifier gain, cut off, and pinhole size across all images. Semi-automated quantification of axon density (Grider et al., 2006) in the lesion area was performed using the open source software Image J and its plug-in Feature J.

BDA-positive axon profiles (with a minimum length of 40 μm) in the lesion area, labeled via BDA-injection into the rostral spinal cord, were quantified by counting them under the microscope. Sections were analyzed using the 10×-objective of a Nikon Diaphot 300 fluorescent microscope. Only BDA-positive structures which could clearly be defined as axons due to specific characteristics (Steward et al., 2003) were taken into account for evaluation.

For the quantification of 5-HT- and TH-positive axon profiles in the spinal cord caudal to the lesion five 40 μm-parasagittal sections from analogous regions were stained for each neurotransmitter and animal. Sections were generally analyzed using the 20×-objective of a Nikon Diaphot 300 fluorescent microscope. Whenever the identification of single axon profiles could not be ensured (*e.g.*, in small entangled axon bundles) the 40×-objective was used for confirmation. Axon profiles were counted under the microscope.

Transmission electron microscopy

For electron microscopic analysis, two operated rats at stage 8 mpr were transcardially perfused as previously described for mice (Groh et al., 2013). Cranial and caudal regions of spinal cords, connected by the grafted area were removed and postfixed in the perfusion fixative, followed by dehydration and embedding in Spurr's resin (Groh et al., 2013). Semithin and serial ultrathin sections were prepared from the caudal end of the cranial spinal cord stump up to 1 mm into the cranial end of the caudal spinal cord, comprising the entire graft area. Sections were collected after every 1–2 mm. Representative ultrathin sections were investigated by a ProScan Slow Scan CCD (ProScan) camera mounted to a Leo 906 E electron microscope (Zeiss) and corresponding software iTEM (Soft Imaging System).

Behavioral testing

Locomotor tests and the subsequent analyses were carried out blinded to the treatment of the animals. Locomotor behavior of animals was assessed weekly using a modified version of the BBB (Basso–Beattie–Bresnahan) score (mBBB) developed by Antri et al. (2002) for complete spinal cord transection. The mBBB expands the locomotor score of the standard BBB open field test that was developed for partial lesions (Basso et al., 1995) in the range of 0–10. However, since the rats in the present study were neither trained nor tested on a treadmill, further modifications of the test procedure and of the mBBB scale as outlined in Supplementary Table 1 were necessary. In lesioned control animals active plantar placement of a hind paw could never be observed, whereas it was occasionally detectable in PEG treated animals. While some of the criteria described by Antri et al. (2002) were never or only rarely observed during locomotor behavior of the animals in our severe chronic SCI studies, other behavioral features were recognized instead, which were not listed in the original publication. An example for the first case is the combination of occasional right–left alteration with large amplitude, no body weight support and occasional plantar foot placement. An example for the latter is the combination of right–left alternation with large amplitude, frequent or consistent body weight support but no active plantar placement of either hind paw. Generally speaking, this resulted in focussing on the animals' body weight support rather than on the rarely observed plantar foot placement in recovery level 4. To evaluate the locomotor outcome the movement of each animal was videotaped in the open field for 4 min, and the recorded videos were subsequently analyzed by visual inspection. For the regular BBB open field testing of animals with partial spinal cord injuries video analyses are not recommended since the scratching noise to detect insufficient toe clearance cannot always unequivocally be recognized on videos (Sedy et al., 2008). However, video recordings in the case of animals with complete transection, which never show toe clearance, are very useful because the animals' over all locomotor behavior can be studied in full detail.

All animals were tested in 5 wpl and were randomly assigned into two groups. TX only-controls ("TX") did not undergo the scar resection procedure, whereas PEG-animals ("PEG") received PEG biopolymer-grafting subsequently to the resection of the TX-scar. Both animal groups ("TX" *vs.* "PEG") initially consisted of N = 14 rats each. One animal ("TX" group) died unexpectedly in post resection-week 27. A second animal ("PEG" group) was sacrificed in post resection-week 18, because it had developed a bladder infection which remained non-responsive to the antibiotic treatment. The spinal cord tissue of the latter animal was included in the axon regeneration analysis.

Blinding procedure

After the initial surgery (partial or complete transection or sham) the animals received a random tail numbering by a third person who kept the key secret. Prior to the second surgery (scar resection) and treatment (biomatrix implantation) of the transected animals, the tail markings were completely covered with Leukoplast (BSN Medical) by the third person so that the surgeon was blinded with regard to the animals' markings. Later the tail markings were removed but the persons who carried out the behavioral testing or the immune histology, respectively, were not aware of the kind of treatment the individual animal had received. After finishing the behavioral and histological analyses the key was broken by the third person. To our understanding this is a double-blind study, since neither the surgeon nor the persons carrying out the subsequent analyses knew the key.

Statistics

All data sets were tested for significant deviations from statistical normality using the Shapiro–Wilk test ($p = 0.05$). Because this test revealed that the distributions of the data were not normal, the non-parametric Kruskal–Wallis test was used for evaluation of significant inter-group differences in axon numbers. Nonparametric tests are better-suited for statistical analyses of data which contain outliers. As

a post hoc test the one-sided Mann–Whitney *U* test was applied for paired comparison and Holm–Bonferroni correction was performed for multiple testing with the type I error rate a = 0.05. The experimental groups were considered significantly different at $p \leq 0.05$.

For the statistical analysis of the behavioral test results of animals with complete spinal transection, a paired comparison was performed using the one-sided Mann–Whitney *U* test. The experimental groups were considered significantly different at $p \leq 0.05$.

For statistical comparison of the mBBB scores of the additional group of PEG ReTX animals prior to and post re-transection, respectively, the Mann–Whitney test was not used because in the case of small samples it has little power to detect small differences. Therefore, the two-sided Kolmogorov–Smirmov test was applied and the values were considered significantly different at $p \leq 0.05$. Unlike Mann–Whitney this test will not rank differences in observation but it can detect differences between means.

Results

Five weeks after initial dorsal hemisection (HX) or complete spinal cord transection (TX) at thoracic level Th8/9, the rats underwent resection of the lesion scar. Aspiration proved to be a suitable method for scar removal in chronic SCI. The scar tissue could be clearly identified by its differing texture and density compared to intact spinal cord. Preparing a longitudinal aspiration cavity of 4 mm in length we made sure that the entire scar tissue plus a small rim of intact spinal cord directly adjacent to the lesion scar was removed. Reproducibility of the scar resection method was verified histologically in a set of animals prior to this study. Possible re-injury of previously cut and retracted axons in the rim was intended to reactivate the neuronal regeneration program including re-stimulation of axon growth which have previously been described for the acute injury situation (Kruse et al., 2011). Animals were sacrificed at either 1 week (for immunohistochemical characterization of the lesion area), 5 weeks (for axon profile quantification) or 8 months (for the analysis of locomotor function improvement) post scar resection (wpr, mpr), respectively.

Comparison of axon profiles in different matrices

Axon growth into the lesion area was assessed by means of immune reactivity (IR) to a neurofilament marker (NF) at 1 wpr (Supplementary Fig. 4) and 5 wpr (Fig. 1) after chronic scar resection. Virtually no or only scarce axonal in-growth into the biopolymer matrix was found in the Matrigel™ (MG) group. Therefore, MG was excluded from further analyses. Only few axon profiles, however, were observed in the center of the ALG-matrix and quantification of NF-positive axon profiles at 5 wpr showed no significant difference between the ALG (Fig. 1B) and the resection only (RX only)-control group (Figs. 1A,D).

The highest axon density was observed in polyethylene glycol 600 (PEG)-treated animals at 1 wpr (Supplementary Fig. 4) and also at 5 wpr (Figs. 1C,D). The axon profiles were evenly distributed within the entire lesion area, including the lesion center, and mostly displayed in bundle-like assemblies. Quantification revealed a 6–7-fold higher axon profile density in PEG (2.4% NF signal area of total matrix filled region) as compared to RX only- (0.34%) or ALG (0.39%)-animals.

To label regenerating axons in the matrix-filled area at 5 wpr, descending spinal axons were anterogradely traced with biotinylated dextran amine (BDA, intraspinal injection 3 mm rostral from lesion site). Only fluorescently stained BDA-labeled structures which could clearly be identified microscopically as elongated axonal profiles were counted (Figs. 2A–F). Quantification revealed similarly low numbers of BDA-labeled axon profiles in the lesion area of control animals (Fig. 2G; 1.7 axon profiles/section) and ALG-treated animals (1.5 axon profiles/section). Interestingly, addition of the iron chelator BPY-DCA that is known to suppress lesion scarring through inhibition of collagen biosynthesis (Hermanns et al., 2001; Klapka et al., 2005; Schiwy et al., 2009) caused an increase of the number of axon profiles within the ALG-matrix reaching 3.5 axon profiles/section. The increase in axon numbers was not significant after Bonferroni correction. The highest number of BDA-labeled axon profiles in the lesion area, however, was observed in PEG-treated animals reaching 15.5 axon profiles/section (Fig. 2G; $^{***}p \leq 0.001$). Notably, axons in the PEG-matrix often grew in long bundles containing several axons (Figs. 2E,F), whereas short solitary axon profiles were mostly observed in the other groups (Figs. 2A–D).

To prove whether the axon growth supporting effect of PEG is selective for a specific axonal subpopulation or a general growth support for different fiber populations, we analyzed four different exemplary fiber systems for their capability to regenerate into the PEG-graft in chronic SCI animals: anterogradely BDA-labeled corticospinal tract (CST), and immune-labeled catecholaminergic axons (tyrosine hydroxylase, TH), serotonergic axons (5-hydroxytryptamine, 5-HT), and ascending sensory fibers (calcitonin gene-related peptide, CGRP). Very interestingly, axons from all fiber populations analyzed were able to grow into the PEG bridge (Fig. 3).

ECM composition, vascularization and cell invasion after biopolymer implantation

ECM composition

The composition of the fibrous scar was investigated via collagen type IV (Col4)-IR. Col4 is one of the major components of basement membrane structures which are enriched in the axon growth inhibitory lesion scar after SCI. The dense extracellular Col4 meshwork which develops at 1 week post lesion (wpl) and is maintained at 5 wpl in lesion only-control animals (Figs. 4A,B) appeared reduced in the matrix area of ALG-treated animals (Fig. 4C). Although some Col4-IR was still detectable in the PEG-biomatrix area, the extracellular Col4 accumulation was markedly diminished in PEG animals compared to the other groups (Fig. 4D). Corresponding to the elevated Col4 accumulation in ALG compared to PEG, a much higher number of prolyl 4-hydroxylase (P-4-H) immunopositive collagen-producing cells was found in ALG- than in PEG-grafts (Figs. 4E–J).

Enhanced vascularization of the PEG-graft

In lesion only-control animals and in the ALG-group small diameter blood vessels (Bv) were sporadically observed at 5 wpl and 1 wpr, respectively (Supplementary Fig. 5). In contrast, PEG-treated animals showed a dense distribution of mostly large diameter Bv throughout the entire matrix area. Numerous large and intensely stained Bv within the PEG-graft often appeared in direct association with NF-positive axon profiles as shown by confocal microscopy. Such close association of Bv with axons could not be detected in any of the other animal groups.

Glial cell invasion and inflammation

In both ALG-and PEG-treated animals APC-immunopositive oligodendroglial cells were absent from the lesion center, but were always detectable at the lesion margin (Supplementary Fig. 6), which is the site of the GFAP-rich *glia limitans*. Additionally, only very few NG2-positive oligodendrocytic precursor cells were detected in the lesion area (Supplementary Fig. 7).

In control animals, the lesion area was virtually devoid of GFAP-positive structures (Supplementary Fig. 8) and remained so for several weeks post lesion (data not shown). In contrast, while ALG-animals showed only a few GFAP-positive, in PEG animals numerous astrocytic processes elongated into the PEG-graft and some GFAP-positive cells resembling astrocytes invaded the graft.

The presence of Schwann cells was assessed via double-immunostaining with GFAP, a protein overexpressed by reactive astrocytes, together with S100, a protein normally present in both Schwann cells as well as in astrocytes (Biernaskie et al., 2007; Casella et al., 2004). Here we observed two S100-positive phenotypes: Cells showing IR for

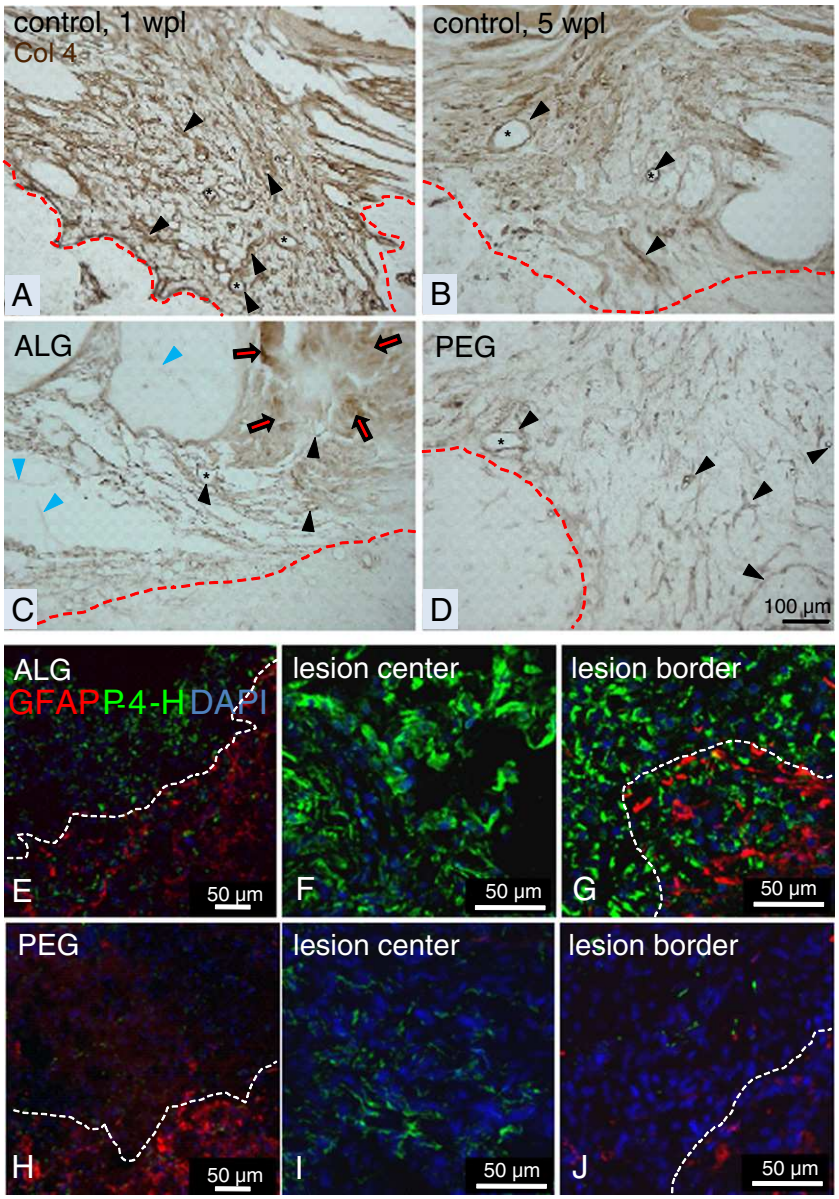

Fig. 4. Deposition of ECM and appearance of prolyl 4-hydroxylase (P-4-H) immunopositive collagen-producing cells in the HX lesion/matrix area. Representative images of Col4-IR visualized via DAB-reaction in the lesion area in 10 µm sagittal sections of lesion only-controls (A + B), and of ALG- (C) and PEG- (D) animals at 1 wpr. Dashed lines delineate lesion area. Note large holes in ALG-matrix, some of which contained sparse ALG-residues (blue arrowheads); red arrows: areas with strong Col4-staining intensity in ALG-matrix; black arrowheads and asterisks indicate structures resembling basement membranes or the lumen of blood vessels, respectively. Furthermore, a substantially higher number of P-4-H-positive cells was detected in border and center regions of ALG- (E–G) compared to PEG-matrix (H–J), corresponding to larger amounts of Col4 present in ALG-matrix.

S100 only, which presumably represent Schwann cells, and cells which were positive for both S100 and GFAP-IR, which are astrocytes. S100-positive/GFAP-negative cells were scarce in the lesion area of controls (Fig. 5A) and virtually absent in the lesion core of ALG-animals at 1 wpr (Fig. 5B). In contrast, numerous S100-positive cells were found throughout the entire PEG-matrix, most of these cells were GFAP-negative (Fig. 5C). Importantly, within the PEG-matrix S100-positive cells were frequently found associated with NF-positive axon profiles (Fig. 5D). This finding could be confirmed by confocal laser microscopy (Figs. 5E–G). Very interestingly, within the PEG-biopolymer-matrix some of the S100-positive cells colocalizing with NF-positive axon profiles clearly showed IR for myelin basic protein (MBP) identifying the S100/MBP-positive cells as Schwann cells (Fig. 5H and confocal image Fig. 5I). GFAP-positive astrocytes were never found as intimately associated with axons in the PEG-matrix as were the S100-positive Schwann cells.

Inflammatory cells were investigated using IR to ED1, a marker for activated macrophages and microglia. In accordance with a chronic inflammatory response after SCI described in the literature (David and Kroner, 2011), the lesion center of control animals was densely packed with ED1-positive cells at all time points (Supplementary Fig. 9A), whereas the centers of ALG- and PEG-grafts were virtually devoid of ED1-IR, but accumulation of ED1-positive cells was found at the lesion borders at 1 wpr. Further immune staining for B- and T-cells revealed very low numbers of the latter cell populations and no obvious differences regarding invasion of the lesion or matrix area, respectively (data not shown).

The analyses revealed that axons, Schwann cells, astrocytes and endothelial cells were present in the PEG-graft, whereas fibroblasts, pericytes, oligodendrocytes and their precursors, B- and T-Cells, and ED1-positive inflammatory cells were only detected in small amounts. Immunohistochemical staining against NG2 further showed that some

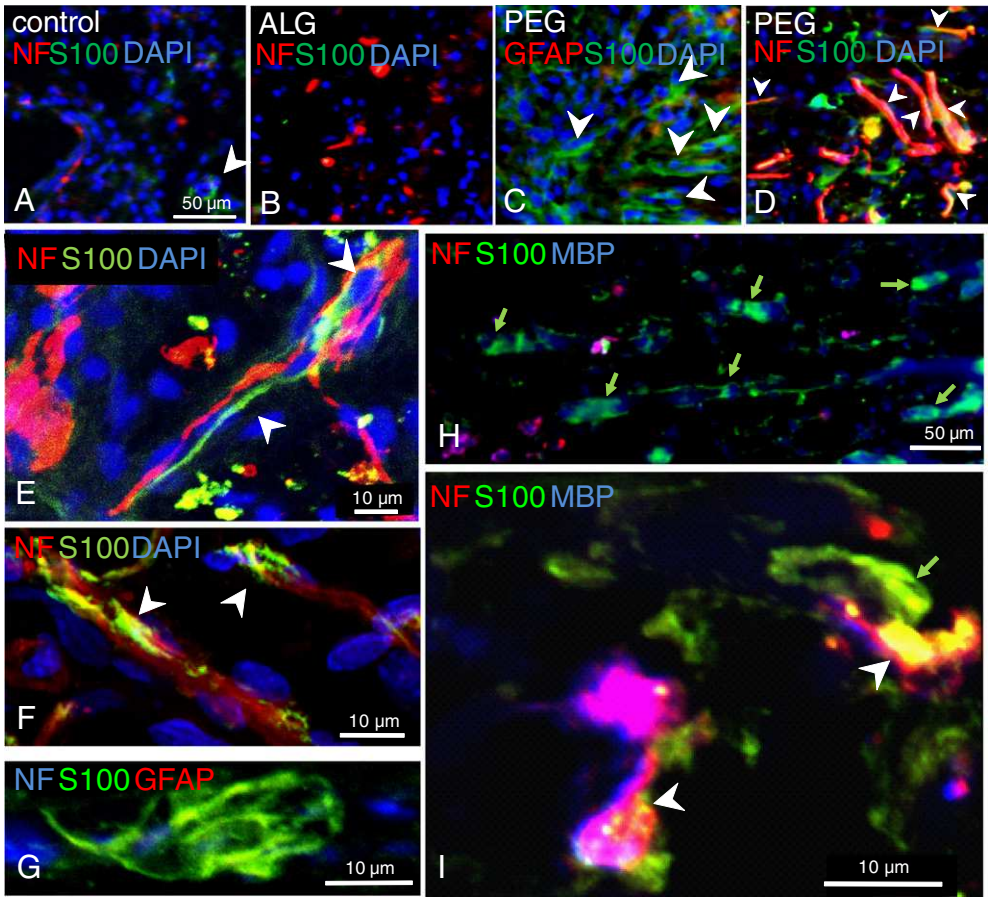

Fig. 5. Cellular invasion of the HX lesion/matrix area with S100β-positive cells and their association with NF-positive axons in PEG. The lesion area of lesion only-controls at 1 wpl (A) and of ALG- (B) or PEG- (C,D) treated animals at 1 wpr was analyzed for cellular invasion. Analyzed cell-types were (GFAP-positive) astrocytes and (S100-positive/GFAP-negative) Schwann cells. Representative images of the lesion/matrix areas in sagittal IF-stained sections are presented. Numerous S100-positive/GFAP-negative cells have invaded the center of the PEG-matrix where they frequently show close association with NF-positive axonal profiles (D). In sagittal sections of the PEG-matrix area NF-positive axon fragments (red in E,F,H,I; blue in G) revealed frequent close associations with S100-positive cells (presumably Schwann cells, green). Some S100 — positive Schwann cells colocalizing with NF-positive axons show immunoreactivity for myelin basic protein MBP (blue MBP-staining in I) suggesting the initiation of myelination. Arrowheads: in (A–D): Schwann cells; in (E, F): very close association of Schwann cells and axons; in (I): association of Schwann cells, myelin and axons. Arrows in (H): MBP-positive Schwann cells; in (I): Schwann cell; 10 µm-sections.

of the cells which are present in the graft at 1 wpr are NG2-positive oligodendrocytic precursor cells (see Supplementary Fig. 7).

Axon regeneration and cell invasion following PEG-grafting in a chronic model of complete SCI

Comparable to PEG-grafting of a chronic moderate HX lesion, analyzed cell populations behaved similarly in the PEG-grafted severe TX lesion site (Supplementary Fig. 10): The GFAP-overexpressing astrocytes of the glial scar elongated into the PEG and formed a loose border between graft and spinal cord tissue. Numerous S100-positive Schwann cells were detected already at 1 wpr, promoting axonal regeneration into the graft.

Additional groups of PEG-treated and lesion (TX)-only control animals (N = 14 each) with a longer survival time of 8 months were analyzed with regard to regenerative axon growth across the grafted area following complete chronic SCI. After 8 months post resection (mpr) axon profiles of different neuronal origins representing both motor (CST, 5-HT, TH) and sensory (CTB-traced dorsal column) fiber systems were not only detected in the lesion area but also in spinal cord areas distal to the lesion and PEG-graft (Figs. 6A–I). Using parasagittal spinal cord sections, quantification of 5-HT and TH immunopositive axon profiles in spinal cord regions beyond the graft revealed highly increased axon profile numbers in PEG-treated animals compared to TX only-controls (Fig. 6 J). The presence of small numbers of axon profiles in the caudal spinal cord of TX only-controls can be explained by the small degree of spontaneous axonal outgrowth as previously described for a dorsal hemisection lesion model (Schiwy et al., 2009), or by axons originating from interneurons, respectively, which have previously been described as one possible source of 5-HT-labeled axons after complete spinal cord transection (Takeoka et al., 2010). Our present results confirm the observation that the lesion scar – although it functions as a robust barrier to regrowing axons – is to some degree permissive for limited spontaneous axon growth which is, however, generally not sufficient to achieve any functional improvement. More animals with long-distance axon growth were observed in the PEG-group than in the controls (Fig. 6 K).

Association of regenerating axons with Schwann cells

Regenerating axons and their associated cells were investigated by transmission electron microscopy (Figs. 7A–F) and immunohistochemistry using laser scanning fluorescence microscopy (Figs. 7G–J). Numerous regenerative fibers were detected in the graft, predominantly associated with basement membrane-forming Schwann cells and Schwann cell-derived myelin ensheathment (Figs. 7A,C,D). Interestingly, axons were organized as "regenerating units" as seen in regenerating peripheral nerves after transection, comprising not only myelinating and non-myelinating Schwann cells, but also fibroblasts, macrophages and "endoneurial" collagen (Figs. 7A,B) (Morris et al., 1972). Astroglial cells could be detected along the entire grafted zone either forming a loose meshwork or a rather dense cellular matrix (Figs. 7B,C)

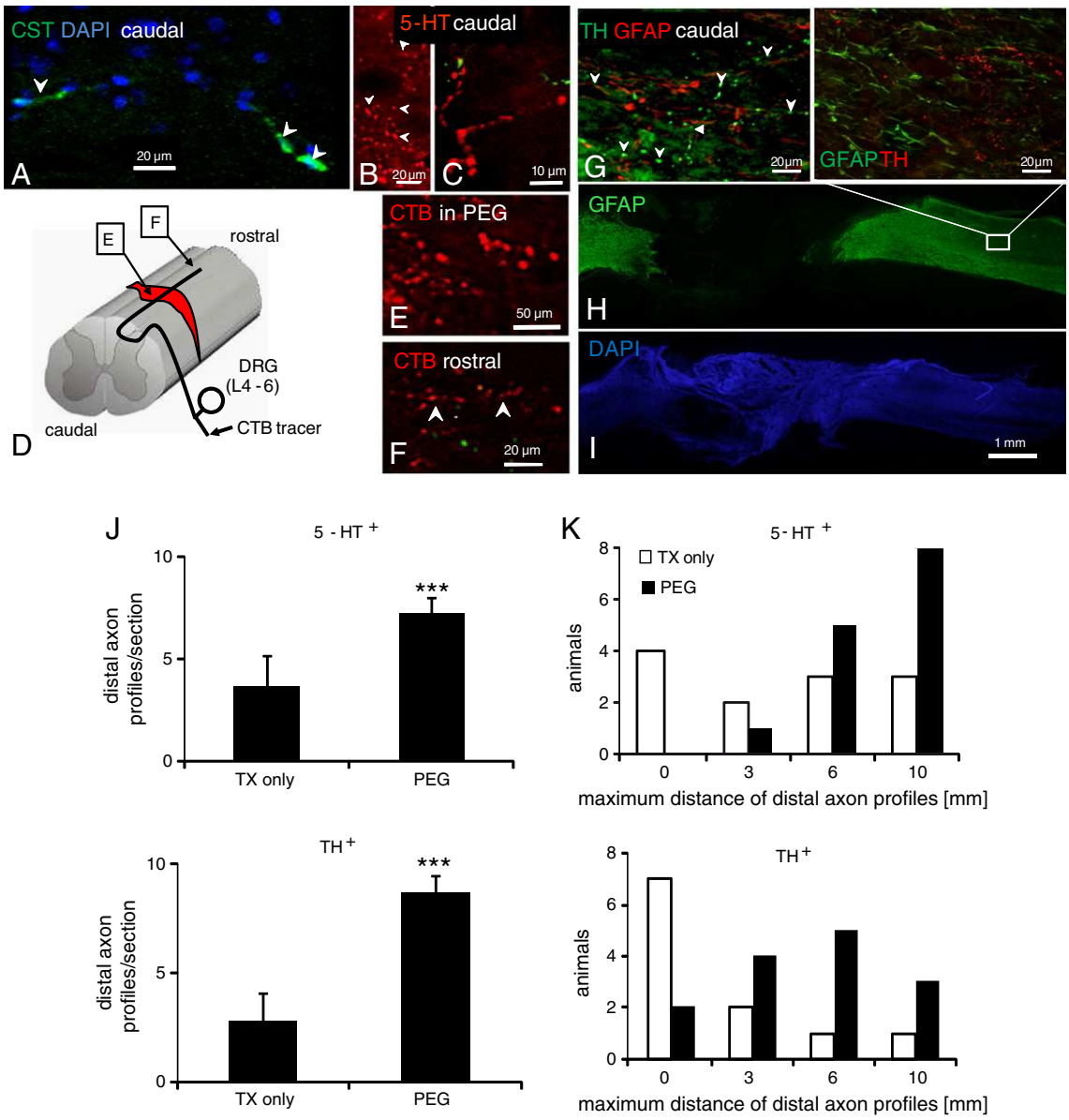

Fig. 6. Long-distance regenerative axon growth in chronic TX SCI animals with PEG-grafts. Regenerative axon growth into and beyond a chronic complete SCI scar removal site filled with PEG 600 was found for all analyzed fiber populations. Examined axonal populations in the PEG-matrix area in sagittal sections were the CST (A), serotonergic (5-HT; B,C) and dopaminergic (TH; G–I) motor axons as well as CTB-labeled sensory axons (E,F). (H,I): Example of TH-positive axon profiles detected 0.5 cm from the lesion center. A schematic drawing of the CTB-tracing procedure and the location of depicted CTB-positive axon profiles is shown in (D). (A): 10 µm-section; (B,C,E–I): 40 µm-sections. Axon fragments were detected in close proximity to the implant area (example in B), but also in very distal parts of the section (example in C: 1 cm distance from the center of the injury). The average length of the sagittal sections was 2 cm with the lesion area located in the section center. The histograms in (J) and (K) represent the quantification and distribution of 5-HT-positive (top panels) and TH-positive axon profiles (bottom panels) in spinal cord areas distal to the site of injury. Significantly increased numbers of both TH-positive and 5-HT-positive axon profiles were detected in PEG-treated animals compared to TX only-controls (J, mean + SEM, one-sided Mann–Whitney *U* test; $^{***}p \leq 0.001$). Bars in (K) represent the distribution of animals according to the maximum distance of their 5-HT-positive (top) and TH-positive axon profiles (bottom) detected in the distal spinal cord. Analysis of the distribution profiles reveals a marked shift towards longer axon growth distances in the PEG-treated animals (n = 14) compared to the TX only-control group (n = 13).

(Frontczak-Baniewicz and Walski, 2006). Typically, when the astrocytic cell matrix had a dense structure the regeneration units appeared as "holes" within this cellular matrix (Fig. 7B). Also, extended meshworks of fibroblastic cells were seen surrounding axon bundles (Fig. 7A). Fibroblastic cells in the PEG-graft which were immunopositive for PDGF receptor alpha (PDGFra, Fig. 7I) but not for PDGFR receptor beta (PDGFrb) are most likely chemotactic stromal fibroblasts (Dong et al., 2004; Osornio-Vargas et al., 1996), whereas those fibroblastic cells in the PEG-graft which were immunopositive for PDGFrb (Fig. 7 J) but not for PDGFRa were considered perivascular fibroblasts/pericytes according to Andrae et al. or Lin et al., respectively (Andrae et al., 2008; Lin et al., 2008). Perivascular cells have recently been described as a major source of fibrotic scar formation after contusive SCI where the dura remains intact (Soderblom et al., 2013). The presence of both chemotactic and perivascular fibroblasts after severe complete TX as observed in our investigation can be explained by the penetrating injury model which involves tearing of the dura. Occasionally, we also observed axon-Schwann cell units that were in association with blood vessels (Fig. 7D), corroborating light microscopic observations using neuronal and vascular markers.

Near the caudal end of the PEG graft close to the border of the distal spinal cord stump regenerated axons with myelin sheaths of

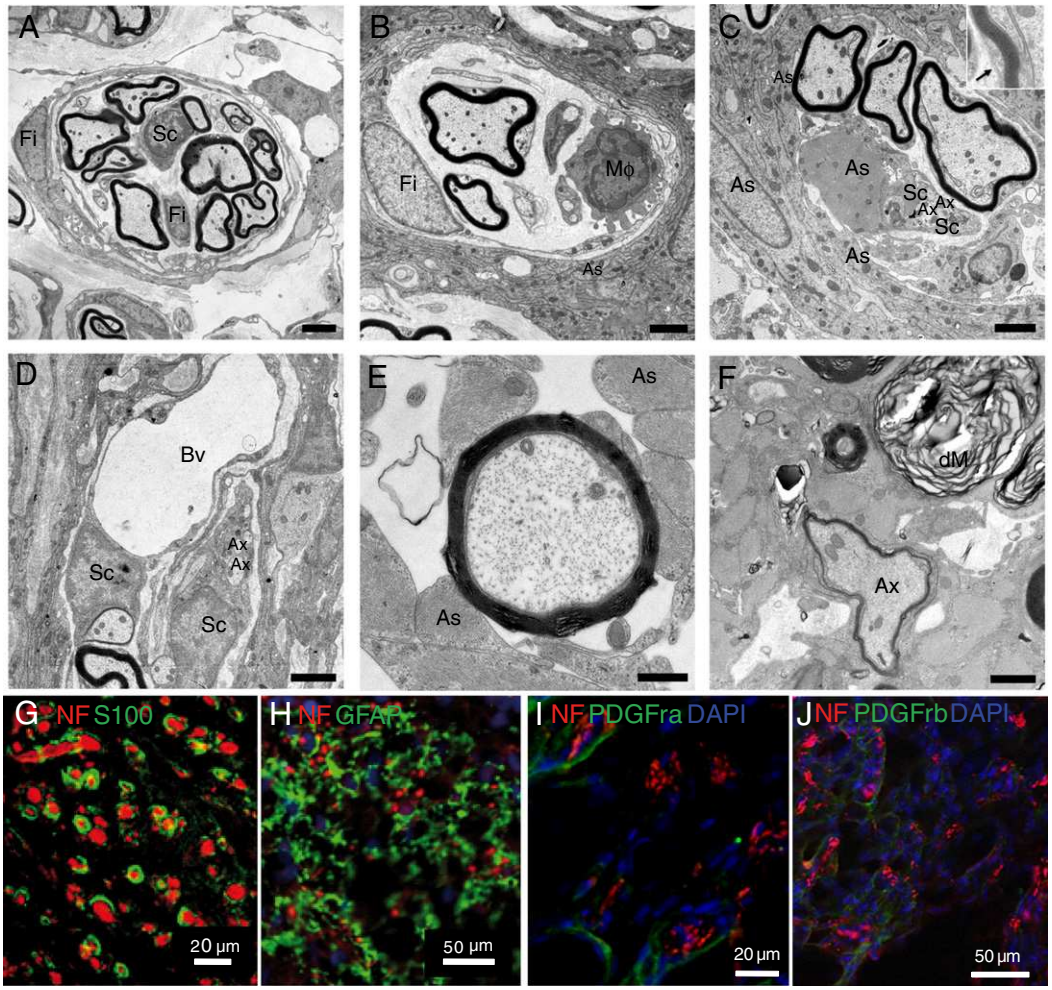

Fig. 7. Transmission electron microscopy and corresponding immunhistological analysis. Electron microscopy of regenerating axons within the grafted TX area (A–E) and within the first millimeter of the caudal part of the transected and PEG-grafted TX spinal cord at 8 mpr. (A, B) Regenerating units within the grafted area comprising axons with Schwann cell-derived myelin sheaths. (A) A regenerating unit is embedded in a loose meshwork of fibroblastic cells (slim cell processes and cellular profiles at the right margin of the micrograph). Other fibroblastic cells (Fi) form a border around the unit or contribute to the "endoneurial" part of the unit. (B) displays a regenerating unit in a dense astrocytic environment (As) and the "endoneurial" part of the unit comprises predominantly myelinating Schwann cells and a macrophage (MΦ). Note that the unit is bordered by a fibroblastic cell (Fi) and that the unit appears as a "hole" in the dense astrocytic matrix. (C) In this situation, the regenerating unit is not as strictly organized as in (A) and (B), since an astrocytic process (As; in the middle of the micrograph) is close to the three axons which are myelinated by Schwann cells. Note that a non-myelinating Schwann cell process (Sc) contacts the astrocytic profile in the middle and that small, regenerating axons (Ax) are in contact with this Schwann cell, but also partly with the astrocyte. Inset: Higher magnification of a myelinating Schwann cell ensheathing the large regenerated axon on the right. The basal lamina (arrow) identifies the myelinating cell as a Schwann cell. (D) Two Schwann cells (Sc) are in close vicinity to a blood vessel (Bv). The left Schwann cell forms a thin myelin sheath around an axon and directly contacts the endothelial cell. The right Schwann cell is associated with thin, regenerating axons (Ax). (E) A regenerated axon – identified by its very thin myelin ensheathment – in the PEG graft close to the caudal part of the spinal cord is surrounded by a myelin sheath of oligodendrocytic origin, as identified by the absence of a basal lamina. Note the abundant astrocytic processes (As). (F) Within the first millimeter of the caudal part of the transected spinal cord, occasionally remnants of oligodendrocytic myelin (dM) reflect the slow Wallerian degeneration after injury 8 months ago. An intact axon (Ax) with a thin, likely recently formed oligodendrocytic myelin sheath possibly identifies this axon as a regenerated one. Bars: 2 µm (A, B, D); 1 µm (C), 0,25 µm (inset in C), and 0.5 µm (E, F). (G–J): IF-stained 10 µm-cross sections of the grafted area. Numerous axons are closely associated with S100-positive Schwann cells (G) in an astrocytic environment (H). Occasionally PDGFra-expressing fibroblasts (I) or PDGFrb-positive perivascular cells (J), respectively, enwrap regenerating units of axons.

oligodendrocytic origin were sometimes observed (Fig. 7E). Typically, the oligodendrocytic sheaths were devoid of a basal lamina and the corresponding axon diameters were usually smaller than those of axons in association with myelinating Schwann cells. The oligodendrocytic myelin sheaths were regularly in close contact to astrocytes, whereas putative oligodendrocytic cell bodies were only rarely seen outside the spinal cord stumps.

Deeper in the spinal cord (approximately 1 mm caudal to the grafted zone) myelin was exclusively formed by oligodendrocytes, as reflected by absence of a basal lamina (Fig. 7 F). Here axons were occasionally seen with proportionally thin but well preserved oligodendrocytic myelin sheaths (Fig. 7 F), possibly representing regenerating axons that successfully bridged the grafted zone and penetrated into the CNS tissue where they became myelinated. Occasional myelin debris likely reflected slow Wallerian degeneration typical for injured CNS tissue (Fig. 7 F).

Locomotor improvement following PEG-application in chronic complete SCI

The locomotor function in animals receiving a chronic dorsal hemisection (HX) in this study was evaluated in an open field using the standard BBB scale (Basso et al., 1995). Due to minor variations in lesion size caused by both initial as well as resection surgery, BBB-results were, however, rather inconsistent which could also possibly be explained by compensatory mechanisms occurring in partial lesions. Therefore, RX-control animals were not included in the long term TX

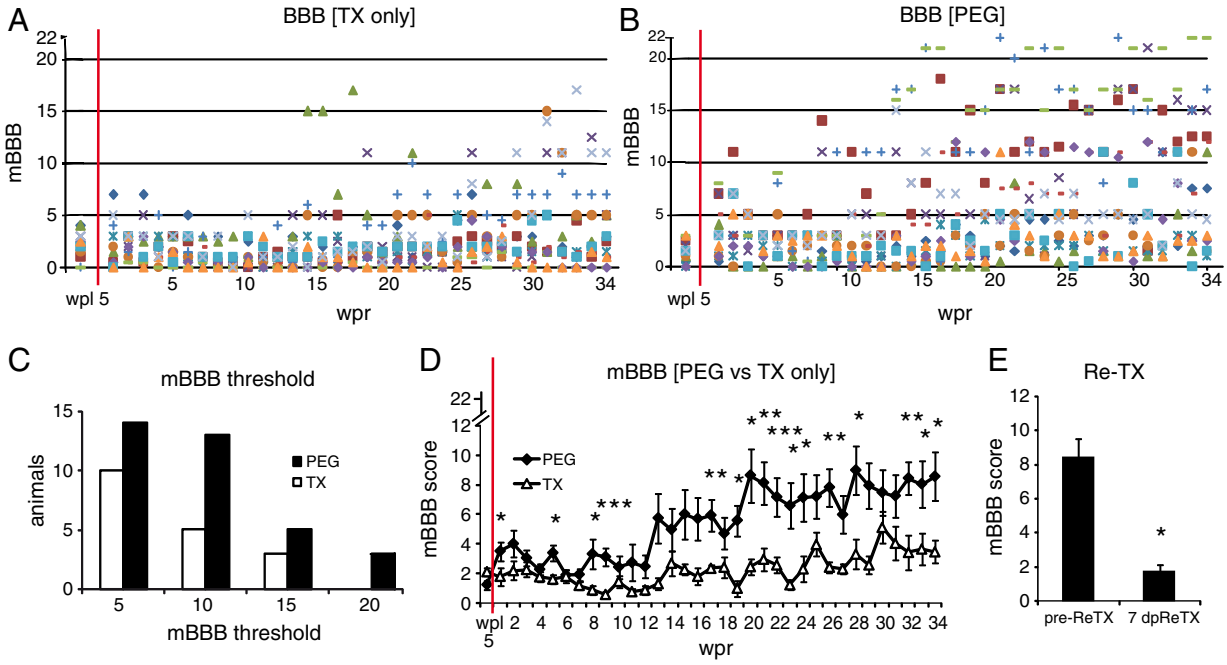

Fig. 8. Functional recovery after PEG-treatment of chronic TX-animals. At all time points more animals of the PEG-group reached higher mBBB scores. (A,B): Scatter plot diagrams showing the individual mBBB scores of lesion only-controls (A) compared to PEG-treated (B) animals per test day. PEG-treated animals revealed significantly better behavioral recovery in the mBBB open field test. Initial early recovery was significantly improved (B), and treated animals generally exhibited higher mBBB-scores than TX-controls (n = 13–14 animals per group per test week); individual animals in (A) and (B) are represented by different colors; (C): Histogram showing the number of animals per group which were able to reach the respective mBBB thresholds. (D): averaged mBBB scores + SEM; one-sided Mann–Whitney *U* test, $^{*}p \leq 0.05$, $^{**}p \leq 0.01$, $^{***}p \leq 0.001$; wpl: weeks post initial lesion; wpr: weeks post resection. Note that for convenience and for better comparability the same time scale is presented for both groups and the time point of resection in wpl 5 is marked by a red line in (A,B and D). However, control animals did not undergo the scar resection procedure. Comparison of the mBBB scores in week 5 post initial lesion (wpl 5) and week one post resection (wpr 1) reveals that the resection procedure did not have any negative effects which could be detected by the mBBB locomotor test. (E): Re-transection (Re-TX) of the spinal cord of n = 3 PEG-treated animals at 8 mpr resulted in significantly reduced mBBB scores, indicating that the observed functional improvement in PEG-treated animals could be the result of the observed regenerative axon growth in these animals; Kolmogorov–Smirnov test, $^{*}p \leq 0.05$.

study because the severe lesion resulted in much more prominent functional deficits and scar resection alone did not prove a successful treatment method. To allow reliable conclusions with respect to functional recovery following PEG-treatment after chronic SCI, the locomotor outcome of animals with a complete chronic spinal cord transection (TX) at thoracic level was evaluated using a modified BBB (mBBB) score (Antri et al., 2002). The mBBB was chosen in order to determine locomotor improvements which are clearly visible to an observer but which would not be reflected by the standard BBB-score, because the standard score was not designed for complete spinal cord injuries. The weekly mBBB scores of animals with complete chronic SCI which received a PEG-graft after scar resection were compared to lesion only (TX)-animals over a period of 8 months. PEG-animals generally revealed higher mBBB-scores than TX-controls (Figs. 8A,B), with significantly higher mean scores in the PEG-group at most time points particularly during long-lasting recovery (Fig. 8D). The data are presented in scatter plots to show all scores of each individual animal. Figs. 8A,B reveal a high degree of variation. Therefore, instead of merely presenting the data as the graph shown in Fig. 8D we believe that it is important to show the heterogeneity because it accounts for both the varying treatment efficacy in different animals and the dependence of the behavioral outcome on the animals' daily condition and motivation on a respective testing day. Clearly, more PEG-treated animals than TX only-controls were able to reach distinct mBBB thresholds increasing stepwise from 5, 10, 15, to 20 (Fig. 8C), respectively. The improved locomotor function in PEG-treated animals with an average mBBB score of 8.5 was significantly diminished to an average score of only 1.8 at 7 days after relesioning (dpReTX, Fig. 8E) indicating a significant contribution of the regenerated and myelinated axons to the improved locomotion in PEG-treated animals.

Discussion

Scar resection and biopolymer-implantation is a potential treatment strategy for chronic SCI

It is generally accepted that none of the experimental procedures to create a spinal cord injury (*e.g.*, weight drop, mechanical transection, balloon compression or clip compression) has a counterpart in human spinal cord trauma (Kim, 2013). For our investigations we chose transection injury models because they lead to reliable results with respect to axonal regeneration. Due to the breached meninges the transection paradigm may be somewhat more scar-promoting than lesion paradigms where the dura remains intact. However, in addition to the induction of large cysts, scar formation has also been described previously as part of the pathology of human spinal cord injuries (Fawcett, 2002), including contusion injuries (Dietz, 2006). We hypothesize that our treatment could also be applied even to chronic SCI models which may comprise less scar formation and more cavity formation because of the resection of the damaged tissue. We have developed a novel treatment paradigm for chronic SCI in rat comprising surgical scar resection and biopolymer-implantation at five weeks after the initial SCI. Tissue integration of the matrices was excellent as no encapsulation of the implant was detected. The overall inflammatory response was less prominent in matrix-implanted than in control-lesioned animals receiving no scar resection.

Since our animal groups which had received a partial SCI showed only a transient drop of 1–3 BBB-score points after scar resection (not shown), we conclude that no additional harm resulting in long-lasting functional deficits is caused by the resection of the scar or damaged tissue. Such animals did, however, reveal an impaired general recovery

compared to matrix-treated animals. RX only-control animals were, therefore, not subject to the prolonged survival periods of the long-term study.

Astrocyte, Schwann cell and endothelial cell invasion but not the entry of prolyl 4-hydroxylase-positive cells into the PEG-biopolymer implant is enhanced

Compared with PEG the ALG-matrix only poorly supported axon growth into and across the lesion area possibly resulting from poor matrix integration of ALG into the host tissue and/or the marginal invasion into the lesion area of cell types known to support regenerative axon growth such as astrocytes, Schwann cells and endothelial cells.

Implantation of PEG after scar removal leads to the formation of a physically stable, growth-supporting biomatrix accompanied by massive elongation and occasional invasion of astrocytes into the resection area. Astrocytes reportedly support axon regeneration providing a suitable growth substrate (White and Jakeman, 2008), and guidance structures (Harel and Strittmatter, 2006; Zhang and Guth, 1997).

Beneficial effects of Schwann cells on axonal regeneration in animal models of SCI are well-known (Oudega, 2007; Pearse et al., 2007). PEG-treated animals not only revealed the highest number of axons within the lesion compared to the other groups, but further showed a marked increase in $S100^{+}/GFAP^{-}$ Schwann cells in this area, whereas the occurrence of such cells was rare in the lesion center of the other animal groups. The latter cells appeared in close contact with regenerating axons.

We further observed a noteworthy degree of angiogenesis within the PEG-biomatrix compared to the other groups. Blood vessels (Bv) in spinal cord have been shown to provide tremendous trophic support for regenerating axons (Rauch et al., 2009) and are important in mediating tissue survival (Peters et al., 2002). Damage of Bv as a consequence of primary injury amplifies secondary lesion events, *e.g.*, disruption of the blood–spinal cord barrier and induction of inflammatory responses (Blight, 1991).

In PEG-implants the least Col4-IR deposition was found compared to fibrotic scar tissue of lesion only-controls and ALG-implants. Corresponding to this, P-4-H-positive cells were abundant in lesion only-controls (not shown) and ALG-treated animals but only rarely detectable in the PEG-matrix. Meningeal fibroblasts or pericyte-derived fibroblastic cells are known to express high levels of P-4-H and are considered the main source for Col4 after SCI (Goritz et al., 2011; Sundberg et al., 1996). As PEG is a neutrally-charged material to which cells or proteins do not generally attach (Gunn et al., 2005), this chemical property could explain the low number of fibroblast infiltrates in the PEG-implant.

PEG-biopolymer supports axon growth

Spontaneous axonal regeneration as visualized by NF-immunohistochemistry and BDA-tracing occurred in all chronically injured animals after scar resection, even in control animals receiving no implant, thus reflecting some very limited regeneration capacity of lesioned neurons. Interestingly, Matrigel™ (MG) proved even to be somewhat repellent to axons, although it has been found to stimulate axonal elongation and reduce axonal dieback when used as a cell carrier substance (Bunge, 2001). The repellent effect of MG when applied as a cell-free substrate confirms previous observations (Bunge, 2002) and might result from axon growth-inhibitory molecules associated with the extracellular matrix, which is an ingredient of MG (Benton et al., 2011). Furthermore, MG-effects are highly variable depending on the batches used (Inman and Bissell, 2010).

On the other hand, we found that ALG allowed some axonal growth, although the effect was not significantly different from controls. Possible growth-promoting effects of ALG might have been hampered by suboptimal tissue integration of ALG-material, which was intently not freeze-dried before use in order to preserve the jelly-like consistency. The low spontaneous axon regeneration into ALG could be increased by the addition of an iron chelator.

By far the best axon growth-support, however, was achieved by implantation of PEG into the lesion cavity. The axon growth effect was visible at 1 wpr and further enhanced at 5 wpr. NF-IR marks most spinal axon subpopulations. Quantification of NF-positive axon profiles resulted in a highly significant 6–7 fold increase of regenerating axons in the PEG-grafted area compared to RX-controls and ALG-treated animals. Previous investigations regarding the biomechanics of axonal growth already indicated that, unlike most other cell types, neurons prefer soft substrates (Flanagan et al., 2002; Georges et al., 2006). Thus, polymer viscosity may be of some importance for both, tissue reformation and axonal regeneration. The previously suggested biophysical mechanism of the fusion of injured axons after acute PEG-application (Borgens et al., 2002; Shi and Borgens, 2000) could not be responsible for the treatment effects in the present lesion paradigm. Detailed analyses of axonal subpopulations in the PEG-implant revealed that the growth-supporting effect is not limited to a single fiber tract. Instead, axons from all tested descending and ascending fiber systems including CST, TH- or 5-HT-containing axons and ascending CGRP-immunopositive as well as CTB-labeled dorsal column axons entered the PEG-implant. Ingrowth of axons from different fiber populations is likely to be mediated by the invading non-neuronal cell populations including, *e.g.*, astrocytes, Schwann cells and endothelial cells that contribute to the formation of a permissive tissue bridge.

Ensheathment of regenerating axons by Schwann cell-derived myelin

By investigating the grafted zone using transmission electron microscopy at 8 mpr, abundant regenerative fibers, predominantly associated with Schwann cell-derived myelin, could be detected. The regenerative fibers were often organized in small fascicles, highly reminiscent of "regenerating units" as seen in regenerating peripheral nerves (Martini et al., 2010; Morris et al., 1972). This would be in line with the observation that the PEG-graft might be particularly attractive or permissive for $S100^{+}/GFAP^{-}$ cells, which we identified as Schwann cells using electron microscopy and confocal laser scanning microscopy. This evokes the question of the origin of the Schwann cells in the PEG-graft. As a response of gliotoxic demyelinating agents, remyelinating, CNS-borne Schwann cells have recently been identified as derivatives of CNS-resident glial progenitor cells (Zawadzka et al., 2010). On the other hand, for the present lesion model, it is plausible to assume that they could be derived from spinal roots that experienced collateral damage or from injured autonomic nerve fibers associated with, *e.g.*, injured blood vessels. Since the regenerating units also comprise other components of the peripheral nervous system, such as endoneurial-like $PDGFra^{+}$ fibroblasts, it is tempting to speculate that these cells are either derived from Schwann cell precursors (Joseph et al., 2004; Richard et al., 2012) or originate from bone marrow, as has been demonstrated by bone marrow transplantation experiments (Maurer et al., 2003). It is unlikely, however, that the majority of fibroblast-like cells represent pericytes since they appear to be $PDGFrb^{-}$.

Significant long-lasting functional locomotor improvement following PEG-treatment in chronic complete SCI

A chronic complete transection injury model and a long survival period were chosen for an extensive (8 months) behavioral analysis. Our results demonstrate that the locomotor behavior of TX-control animals was slightly improved over time which also corresponds with the finding of regenerated axon profiles in the caudal spinal cord of these animals. The results of the open field test reveal that the PEG-matrix allows significant and long-lasting hind limb motor recovery which was still steadily increasing at the end of the time period of the experiment. The average mBBB score of 8.5 which was achieved in chronic

complete thoracic SCI by PEG grafting-only conforms to a BBB score of 8 in the regular BBB. The data further show that PEG-treated animals could reach mBBB scores between 10 (corresponding to BBB 9, n = 13) and even up to 20 (corresponding to BBB 10, n = 2) after chronic complete SCI. Recently, recovery rates after acute and subacute complete thoracic spinal cord transection have been reported with BBB scores of 3 (Bai et al., 2010) and 7 (Lu et al., 2012), respectively. In the latter study BBB scores of 7 were achieved after a combinatorial treatment using neural stem cell-grafts embedded in a fibrin-matrix (Lu et al., 2012). The functional locomotor analysis in the present study revealed that the beneficial effects of the PEG-implant are not temporary but long-lasting. The functional improvement could be explained by the favorable modulation of the PEG-grafted area and the resulting very abundant axon ingrowth into the biomatrix, the long-distance axon regeneration beyond the PEG-graft and the compact myelination of regenerating axons as a prerequisite for fast signal propagation. The important functional contribution of the regenerated axons is further confirmed by disappearance of the observed locomotor improvement in PEG-treated animals following spinal re-transection.

Conclusion

The present investigation in a severe chronic SCI model in rat provides strong evidence for the potential of chronically injured axons of various neuronal origins to regenerate into a PEG-filled scar resection area. Very importantly, the treatment leads to significantly improved, long-lasting hind limb locomotor function. We also demonstrate that PEG implantation into the chronically injured spinal cord results in beneficial cell invasion (Schwann cells, endothelial cells, astrocytes) and elongation (astrocytes). EM-analysis confirmed the histological results and revealed myelin ensheathment of axons in the resection area. Therefore, PEG 600 is an ideal and immunologically inert biopolymer grafting material to improve regeneration and achieve functional recovery in severe chronic SCI and could be further used as a treatment option in combination with other therapeutic strategies for SCI.

We further provide the first direct comparison of Matrigel™, alginate-hydrogel and polyethylene glycol 600 as biopolymers in chronic SCI models. The results demonstrate the remarkable potential of chronically injured spinal cord axons to spontaneously regenerate into a suitable matrix inserted into a cavity resulting from resection of the inhibitory lesion scar.

Supplementary data to this article can be found online at http://dx.doi.org/10.1016/j.nbd.2014.03.018.

Acknowledgments

The authors are grateful to Marion Hendricks and Dennis Klein for the technical help.

This work was supported by grants from the German Paraplegia Foundation (Title: Regeneration nach chronischer Rückenmarkverletzung) and the Research Commission of the Medical Faculty of the Heinrich-Heine-University Düsseldorf (Project 47/2011, Dr. Estrada). Part of the work carried out in the laboratory of R.M. was supported by the German Research Foundation (MA 1053/6-1) and by local funds of the University of Würzburg (IZKF A-168). The funding sources had no direct involvement in the study.

References

Andrae, J., Gallini, R., Betsholtz, C., 2008. Role of platelet-derived growth factors in physiology and medicine. Genes Dev. 22, 1276–1312.
Antri, M., Orsal, D., Barthe, J.Y., 2002. Locomotor recovery in the chronic spinal rat: effects of long-term treatment with a 5-HT2 agonist. Eur. J. Neurosci. 16, 467–476.
Bai, F., Peng, H., Etlinger, J.D., Zeman, R.J., 2010. Partial functional recovery after complete spinal cord transection by combined chondroitinase and clenbuterol treatment. Pflugers Arch. 460, 657–666.
Basso, D.M., Beattie, M.S., Bresnahan, J.C., 1995. A sensitive and reliable locomotor rating scale for open field testing in rats. J. Neurotrauma 12, 1–21.
Benton, G., Kleinman, H.K., George, J., Arnaoutova, I., 2011. Multiple uses of basement membrane-like matrix (BME/Matrigel) in vitro and in vivo with cancer cells. Int. J. Cancer 128, 1751–1757.
Biernaskie, J., Sparling, J.S., Liu, J., Shannon, C.P., Plemel, J.R., Xie, Y., Miller, F.D., Tetzlaff, W., 2007. Skin-derived precursors generate myelinating Schwann cells that promote remyelination and functional recovery after contusion spinal cord injury. J. Neurosci. 27, 9545–9559.
Blight, A.R., 1991. Morphometric analysis of blood vessels in chronic experimental spinal cord injury: hypervascularity and recovery of function. J. Neurol. Sci. 106, 158–174.
Borgens, R.B., Shi, R., Bohnert, D., 2002. Behavioral recovery from spinal cord injury following delayed application of polyethylene glycol. J. Exp. Biol. 205, 1–12.
Buchli, A.D., Schwab, M.E., 2005. Inhibition of Nogo: a key strategy to increase regeneration, plasticity and functional recovery of the lesioned central nervous system. Ann. Med. 37, 556–567.
Bundesen, L.Q., Scheel, T.A., Bregman, B.S., Kromer, L.F., 2003. Ephrin-B2 and EphB2 regulation of astrocyte–meningeal fibroblast interactions in response to spinal cord lesions in adult rats. J. Neurosci. 23, 7789–7800.
Bunge, M.B., 2001. Bridging areas of injury in the spinal cord. Neuroscientist 7, 325–339.
Bunge, M.B., 2002. Bridging the transected or contused adult rat spinal cord with Schwann cell and olfactory ensheathing glia transplants. Prog. Brain Res. 137, 275–282.
Cafferty, W.B., Strittmatter, S.M., 2006. The Nogo–Nogo receptor pathway limits a spectrum of adult CNS axonal growth. J. Neurosci. 26, 12242–12250.
Casella, G.T., Bunge, M.B., Wood, P.M., 2004. Improved immunocytochemical identification of neural, endothelial, and inflammatory cell types in paraffin-embedded injured adult rat spinal cord. J. Neurosci. Methods 139, 1–11.
Cassell, O.C., Morrison, W.A., Messina, A., Penington, A.J., Thompson, E.W., Stevens, G.W., Perera, J.M., Kleinman, H.K., Hurley, J.V., Romeo, R., Knight, K.R., 2001. The influence of extracellular matrix on the generation of vascularized, engineered, transplantable tissue. Ann. N. Y. Acad. Sci. 944, 429–442.
David, S., Kroner, A., 2011. Repertoire of microglial and macrophage responses after spinal cord injury. Nat. Rev. Neurosci. 12, 388–399.
Davies, J.E., Tang, X., Denning, J.W., Archibald, S.J., Davies, S.J., 2004. Decorin suppresses neurocan, brevican, phosphacan and NG2 expression and promotes axon growth across adult rat spinal cord injuries. Eur. J. Neurosci. 19, 1226–1242.
Dietz, V., 2006. G. Heiner sell memorial lecture: neuronal plasticity after spinal cord injury: significance for present and future treatments. J. Spinal Cord Med. 29 (5), 481–488.
Dong, J., Grunstein, J., Tejada, M., Peale, F., Frantz, G., Liang, W.C., Bai, W., Yu, L., Kowalski, J. , Liang, X., Fuh, G., Gerber, H.P., Ferrara, N., 2004. VEGF-null cells require PDGFR alpha signaling-mediated stromal fibroblast recruitment for tumorigenesis. EMBO J. 23, 2800–2810.
European Food Safety Authority, 2006. Opinion of the Scientific Panel on Food Additives, Flavourings, Processing Aids and Materials in Contact with Food on a Request from the Commission Related to an Application on the Use of Polyethylene Glycol (PEG) as a Film Coating Agent for Use in Food Supplement Products — QUESTION N° EFSA-Q-2005-277. EFSA J. http://www.efsa.europa.eu/en/scdocs/doc/afc_op_ej414_polyethylene_glycol_sum_en%20,0.pdf.
Fawcett, J., 2002. Repair of spinal cord injuries: where are we, where are we going? Spinal Cord 40, 615–623.
Fawcett, J.W., 2006. The glial response to injury and its role in the inhibition of CNS repair. Adv. Exp. Med. Biol. 557, 11–24.
Filbin, M.T., 2003. Myelin-associated inhibitors of axonal regeneration in the adult mammalian CNS. Nat. Rev. Neurosci. 4, 1–11.
Flanagan, L.A., Ju, Y.E., Marg, B., Osterfield, M., Janmey, P.A., 2002. Neurite branching on deformable substrates. Neuroreport 13, 2411–2415.
Frontczak-Baniewicz, M., Walski, M., 2006. Glial scar instability after brain injury. J. Physiol. Pharmacol. 57 (Suppl. 4), 97–102.
Georges, P.C., Miller, W.J., Meaney, D.F., Sawyer, E.S., Janmey, P.A., 2006. Matrices with compliance comparable to that of brain tissue select neuronal over glial growth in mixed cortical cultures. Biophys. J. 90, 3012–3018.
Goritz, C., Dias, D.O., Tomilin, N., Barbacid, M., Shupliakov, O., Frisen, J., 2011. A pericyte origin of spinal cord scar tissue. Science 333, 238–242.
Grider, M.H., Chen, Q., Shine, H.D., 2006. Semi-automated quantification of axonal densities in labeled CNS tissue. J. Neurosci. Methods 155, 172–179.
Groh, J., Kuhl, T.G., Ip, C.W., Nelvagal, H.R., Sri, S., Duckett, S., Mirza, M., Langmann, T., Cooper, J.D., Martini, R., 2013. Immune cells perturb axons and impair neuronal survival in a mouse model of infantile neuronal ceroidlipofuscinosis. Brain 136, 1083–1101.
Gunn, J.W., Turner, S.D., Mann, B.K., 2005. Adhesive and mechanical properties of hydrogels influence neurite extension. J. Biomed. Mater. Res. A 72, 91–97.
Harel, N.Y., Strittmatter, S.M., 2006. Can regenerating axons recapitulate developmental guidance during recovery from spinal cord injury? Nat. Rev. Neurosci. 7, 603–616.
Hermanns, S., Reiprich, P., Muller, H.W., 2001. A reliable method to reduce collagen scar formation in the lesioned rat spinal cord. J. Neurosci. Methods 110, 141–146.
Houle, J.D., Tessler, A., 2003. Repair of chronic spinal cord injury. Exp. Neurol. 182, 247–260.
Inman, J.L., Bissell, M.J., 2010. Apical polarity in three-dimensional culture systems: where to now? J. Biol. 9, 2.
Joseph, N.M., Mukouyama, Y.S., Mosher, J.T., Jaegle, M., Crone, S.A., Dormand, E.L., Lee, K.F., Meijer, D., Anderson, D.J., Morrison, S.J., 2004. Neural crest stem cells undergo multilineage differentiation in developing peripheral nerves to generate endoneurial fibroblasts in addition to Schwann cells. Development 131, 5599–5612.

Kataoka, K., Suzuki, Y., Kitada, M., Hashimoto, T., Chou, H., Bai, H., Ohta, M., Wu, S., Suzuki, K., Ide, C., 2004. Alginate enhances elongation of early regenerating axons in spinal cord of young rats. Tissue Eng. 10, 493–504.

Kim, R.C., 2013. The pathological findings in traumatic injury to the human spinal cord. In: Aldskogius, Håkan (Ed.), Animal Models of Spinal Cord RepairNeuromethods 76, 25–37.

Klapka, N., Muller, H.W., 2006. Collagen matrix in spinal cord injury. J. Neurotrauma 23, 422–435.

Klapka, N., Hermanns, S., Straten, G., Masanneck, C., Duis, S., Hamers, F.P., Muller, D., Zuschratter, W., Muller, H.W., 2005. Suppression of fibrous scarring in spinal cord injury of rat promotes long-distance regeneration of corticospinal tract axons, rescue of primary motoneurons in somatosensory cortex and significant functional recovery. Eur. J. Neurosci. 22, 3047–3058.

Kruse, F., Bosse, F., Vogelaar, C.F., Brazda, N., Kury, P., Gasis, M., Muller, H.W., 2011. Cortical gene expression in spinal cord injury and repair: insight into the functional complexity of the neural regeneration program. Front. Mol. Neurosci. 4, 26.

Lin, S.L., Kisseleva, T., Brenner, D.A., Duffield, J.S., 2008. Pericytes and perivascular fibroblasts are the primary source of collagen-producing cells in obstructive fibrosis of the kidney. Am. J. Pathol. 173, 1617–1627.

Lu, P., Wang, Y., Graham, L., McHale, K., Gao, M., Wu, D., Brock, J., Blesch, A., Rosenzweig, E. S., Havton, L.A., Zheng, B., Conner, J.M., Marsala, M., Tuszynski, M.H., 2012. Long-distance growth and connectivity of neural stem cells after severe spinal cord injury. Cell 150, 1264–1273.

Martini, R., Groh, J., Bartsch, U., 2010. Comparative biology of Schwann cells and oligodendrocytes. In: Armati, P.J., Mathey, E.K. (Eds.), The Biology of Oligodendrocytes. Cambridge University Press, Cambridge, pp. 19–48.

Maurer, M., Muller, M., Kobsar, I., Leonhard, C., Martini, R., Kiefer, R., 2003. Origin of pathogenic macrophages and endoneurial fibroblast-like cells in an animal model of inherited neuropathy. Mol. Cell. Neurosci. 23, 351–359.

Morris, J.H., Hudson, A.R., Weddell, G., 1972. A study of degeneration and regeneration in the divided rat sciatic nerve based on electron microscopy. II. The development of the "regenerating unit". Z. Zellforsch. Mikrosk. Anat. 124, 103–130.

Niclou, S.P., Ehlert, E.M., Verhaagen, J., 2006. Chemorepellent axon guidance molecules in spinal cord injury. J. Neurotrauma 23, 409–421.

Novikov, L.N., Novikova, L.N., Mosahebi, A., Wiberg, M., Terenghi, G., Kellerth, J.O., 2002. A novel biodegradable implant for neuronal rescue and regeneration after spinal cord injury. Biomaterials 23, 3369–3376.

Novikova, L.N., Mosahebi, A., Wiberg, M., Terenghi, G., Kellerth, J.O., Novikov, L.N., 2006. Alginate hydrogel and matrigel as potential cell carriers for neurotransplantation. J. Biomed. Mater. Res. A 77 (2), 242–252 (May).

Osornio-Vargas, A.R., Lindroos, P.M., Coin, P.G., Badgett, A., Hernandez-Rodriguez, N.A., Bonner, J.C., 1996. Maximal PDGF-induced lung fibroblast chemotaxis requires PDGF receptor-alpha. Am. J. Physiol. 271, L93–L99.

Oudega, M., 2007. Schwann cell and olfactory ensheathing cell implantation for repair of the contused spinal cord. Acta Physiol. (Oxf.) 189, 181–189.

Pearse, D.D., Sanchez, A.R., Pereira, F.C., Andrade, C.M., Puzis, R., Pressman, Y., Golden, K., Kitay, B.M., Blits, B., Wood, P.M., Bunge, M.B., 2007. Transplantation of Schwann cells and/or olfactory ensheathing glia into the contused spinal cord: survival, migration, axon association, and functional recovery. Glia 55, 976–1000.

Peters, M.C., Polverini, P.J., Mooney, D.J., 2002. Engineering vascular networks in porous polymer matrices. J. Biomed. Mater. Res. 60, 668–678.

Rauch, M.F., Hynes, S.R., Bertram, J., Redmond, A., Robinson, R., Williams, C., Xu, H., Madri, J.A., Lavik, E.B., 2009. Engineering angiogenesis following spinal cord injury: a coculture of neural progenitor and endothelial cells in a degradable polymer implant leads to an increase in vessel density and formation of the blood–spinal cord barrier. Eur. J. Neurosci. 29, 132–145.

Richard, L., Topilko, P., Magy, L., Decouvelaere, A.V., Charnay, P., Funalot, B., Vallat, J.M., 2012. Endoneurial fibroblast-like cells. J. Neuropathol. Exp. Neurol. 71, 938–947.

Schiwy, N., Brazda, N., Muller, H.W., 2009. Enhanced regenerative axon growth of multiple fibre populations in traumatic spinal cord injury following scar-suppressing treatment. Eur. J. Neurosci. 30, 1544–1553.

Sedy, J., Urdzikova, L., Jendelova, P., Sykova, E., 2008. Methods for behavioral testing of spinal cord injured rats. Neurosci. Biobehav. Rev. 32, 550–580.

Shi, R., Borgens, R.B., 2000. Anatomical repair of nerve membranes in crushed mammalian spinal cord with polyethylene glycol. J. Neurocytol. 29, 633–643.

Silver, J., Miller, J.H., 2004. Regeneration beyond the glial scar. Nat. Rev. Neurosci. 5, 146–156.

Soderblom, C., Luo, X., Blumenthal, E., Bray, E., Lyapichev, K., Ramos, J., Krishnan, V., Lai-Hsu, C., Park, K.K., Tsoulfas, P., Lee, J.K., 2013. Perivascular fibroblasts form the fibrotic scar after contusive spinal cord injury. J. Neurosci. 33, 13882–13887.

Steward, O., Zheng, B., Tessier-Lavigne, M., 2003. False resurrections: distinguishing regenerated from spared axons in the injured central nervous system. J. Comp. Neurol. 459, 1–8.

Sundberg, C., Ivarsson, M., Gerdin, B., Rubin, K., 1996. Pericytes as collagen-producing cells in excessive dermal scarring. Lab. Invest. 74, 452–466.

Takeoka, A., Kubasak, M.D., Zhong, H., Kaplan, J., Roy, R.R., Phelps, P.E., 2010. Noradrenergic innervation of the rat spinal cord caudal to a complete spinal cord transection: effects of olfactory ensheathing glia. Exp. Neurol. 222, 59–69.

Tang, X., Davies, J.E., Davies, S.J., 2003. Changes in distribution, cell associations, and protein expression levels of NG2, neurocan, phosphacan, brevican, versican V2, and tenascin-C during acute to chronic maturation of spinal cord scar tissue. J. Neurosci. Res. 71, 427–444.

Tonge, D.A., Golding, J.P., Edbladh, M., Kroon, M., Ekstrom, P.E., Edstrom, A., 1997. Effects of extracellular matrix components on axonal outgrowth from peripheral nerves of adult animals in vitro. Exp. Neurol. 146, 81–90.

Ung, R.V., Lapointe, N.P., Tremblay, C., Larouche, A., Guertin, P.A., 2007. Spontaneous recovery of hindlimb movement in completely spinal cord transected mice: a comparison of assessment methods and conditions. Spinal Cord 45, 367–379.

White, R.E., Jakeman, L.B., Tessier-Lavigne, M., 2008. Don't fence me in: harnessing the beneficial roles of astrocytes for spinal cord repair. Restor Neurol Neurosci. 26, 197–214.

Zawadzka, M., Rivers, L.E., Fancy, S.P., Zhao, C., Tripathi, R., Jamen, F., Young, K., Goncharevich, A., Pohl, H., Rizzi, M., Rowitch, D.H., Kessaris, N., Suter, U., Richardson, W.D., Franklin, R.J., 2010. CNS-resident glial progenitor/stem cells produce Schwann cells as well as oligodendrocytes during repair of CNS demyelination. Cell Stem Cell 6, 578–590.

Zhang, Z., Guth, L., Tessier-Lavigne, M., 1997. Experimental spinal cord injury: Wallerian degeneration in the dorsal column is followed by revascularization, glial proliferation, and nerve regeneration. Exp Neurol. 147, 159–171.